

Investigation of unintentional indium incorporation into GaN barriers of InGaN/GaN quantum well structures

F. C.-P. Massabuau^{*1}, M. J. Davies², W. E. Blenkhorn², S. Hammersley², M. J. Kappers¹, C. J. Humphreys¹, P. Dawson², and R. A. Oliver¹

¹ Department of Materials Science and Metallurgy, University of Cambridge, Cambridge, UK


² School of Physics and Astronomy, Photon Science Institute, University of Manchester, Manchester, UK

Received 22 September 2014, revised 5 November 2014, accepted 6 November 2014

Published online 22 December 2014

Keywords GaN, indium, InGaN, quantum wells, segregation, transmission electron microscopy

* Corresponding author: e-mail fm350@cam.ac.uk, Phone: +44 1223 334044, Fax: +44 1223 334437

 This is an open access article under the terms of the Creative Commons Attribution License, which permits use, distribution and reproduction in any medium, provided the original work is properly cited.

High resolution transmission electron microscopy has been employed to investigate the impact of the GaN barrier growth technique on the composition profile of InGaN quantum wells (QWs). We show that the profiles deviate from their nominal configuration due to the presence of an indium tail at the upper interface of the QW. This indium tail, thought to be associated with a segregation effect from the indium surfactant layer, has been shown to strongly depend on the growth method. The effect of this tail has been investigated using a self-consistent Schrödinger–Poisson simulation. For the simulated conditions,

a graded upper interface has been found to result in a decreased electron-hole wavefunction overlap of up to 31% compared to a QW with a rectangular profile, possibly leading to a decrease in radiative-recombination rate. Therefore, in order to maximize the efficiency of a QW structure, it is important to grow the active region using a growth method which leads to QW interfaces which are as abrupt as possible. The results of this experiment find applications in every study where the emission properties of a device are correlated to a particular active region design.

1 Introduction InGaN/GaN quantum wells (QWs) are widely used for making optoelectronic devices such as light emitting diodes (LEDs) [1, 2]. In recent years, significant research effort has been put into optimizing the structure of LEDs in order to reduce efficiency droop, the quantum confined Stark effect (QCSE), etc. One of the main focuses of such studies was to investigate how the indium composition profile of the InGaN QWs impacts the LED efficiency [3–5]. A second aspect, somewhat related to the former, was to investigate the effect of the GaN barrier growth method [6, 7] on the performance of LEDs.

In studying the indium composition profile of the InGaN wells, a wide range of shapes have been investigated, including rectangular (the most commonly utilized profile), triangular [3, 5], graded upper interfaces [3] and smooth step-like QW interfaces [4]. It was then claimed that such profiles would affect the sensitivity to the QCSE [5], the electron-hole wavefunction overlap [3, 5] or the Auger recombination rate [4, 8]. However most of these studies, whether theoretical or experimental, assume that the

composition profile of the QW is defined by the growth recipe used for the QW. For instance a nominally rectangular QW, as is typically grown in most devices, is assumed to have perfectly abrupt GaN/InGaN and InGaN/GaN interfaces. However, experimental observations of deviations from the nominally grown profile have been reported [6, 9–11]. It has been shown that the growth of a nominally rectangular QW with high indium content (nominally 25–30% indium) results in a graded InGaN/GaN interface, due to unintentional indium incorporation in the GaN barrier. The compositional profile showed either a decay [6, 9] or a plateau of indium [10, 11] inside the GaN barrier. These deviations should be considered when one is investigating how the QW profile affects the emission properties of a device. For instance Yakovlev et al. [6] simulated the impact of the barrier temperature on the composition profile and efficiency of a high indium InGaN/GaN superlattice with nominally rectangular QWs and showed that the penetration of indium into the barrier (itself strongly related to the GaN growth temperature) noticeably affected the device

performance [6]. However, the simulation they presented did not take into account the desorption of indium from the QW which occurs during any growth interruption or exposure to high temperatures, which may lead to gross well-width fluctuations (GWWFs) [12]. These studies suggest that the QW composition profile, GaN barrier growth conditions and device performance are strongly interconnected, but also show that there is a hiatus between theories based on nominal growth recipes, and physical reality.

In this study, we have employed high resolution transmission electron microscopy (HRTEM) to investigate the structure of blue-emitting InGaN/GaN QWs grown by metal-organic vapor phase epitaxy (MOVPE) with various barrier growth treatments. We observe the unintentional incorporation of indium into the barrier material and we show that the barrier growth method strongly affects the QW profile. The incorporation of indium into the GaN barrier results in an exponential decay of the indium composition at the upper InGaN/GaN interface. The impact of such features on the band structure and luminescence properties of the device are investigated using a self-consistent Schrödinger–Poisson calculator [13].

2 Experimental methods Four ten-period InGaN/GaN QW structures were grown by MOVPE in a Thomas Swan 6×2 inch showerhead reactor. Trimethylgallium (TMG), trimethylindium (TMI) and ammonia (NH_3) were used as precursors for Ga, In and N, respectively. Hydrogen (H_2) was used as the carrier gas for GaN growth and nitrogen (N_2) as the carrier gas for InGaN growth. Pseudo-substrates consisting of ca. $5 \mu\text{m}$ of GaN (of which $2 \mu\text{m}$ undoped and $3 \mu\text{m}$ Si-doped to $5 \times 10^{18} \text{cm}^{-3}$) grown on c -plane sapphire with a miscut of $(0.25 \pm 0.1)^\circ$ towards $(11\bar{2}0)$ were employed. The four samples were grown using four different growth techniques which we refer to as 1T, Q2T, \sim Q2T and 2T (See Fig. 1). For the 1T sample, following the growth of a nominally 2.5 nm InGaN QW at 756°C , the entire GaN barrier is grown at the same temperature. For the Q2T sample, a ca. 1 nm thin protective GaN cap layer is grown on

top of the QW before ramping the temperature to 860°C , during which an additional 1 nm of GaN is being deposited. The growth of GaN goes on whilst the temperature is maintained at 860°C until a total of ca. 7.5 nm of GaN has been deposited. For the \sim Q2T sample, the temperature is ramped to 860°C right after the InGaN QW is grown at 756°C . Approximately 1 nm of GaN is grown during the temperature ramp and the remaining GaN is grown at 860°C . For the 2T sample, to compensate any loss of indium during the temperature ramp, the QW is grown at 747°C , and the temperature is increased directly after the InGaN is grown. The growth of the barrier starts when the temperature has reached 852°C to settle at 860°C .

The composition and thickness of the QW structures were determined by X-ray diffraction (XRD) using Vickers et al.'s method [14], and are summarized in Table 1. HRTEM was used to conduct a geometric phase analysis using a JEOL 4000EX [15]. High angular annular dark field scanning transmission electron microscopy (STEM-HAADF) was also performed using an FEI Tecnai F20 and an FEI Tecnai Osiris. The band structure of the samples was simulated using a self-consistent Schrödinger–Poisson calculator [13].

The geometric phase analysis was performed as follows; HRTEM images were taken under symmetric three-beam conditions, including beams $g = 0002$, $g = 0$ and $g = 0002$, resulting in interference fringes parallel to the growth plane, and with a spacing related to the c -lattice parameter of the material. The images were then filtered using a 20 cycles Wiener filter. Because a hard mask would create ripples in the deformation map, a Gaussian mask with a radius of $\frac{g}{3}$ and a cut-off of $\frac{g}{2}$ was centered on $g = 0002$. Geometric phase analysis, resulting in a $\varepsilon_z = (c - c_{\text{ref}})/c_{\text{ref}}$ deformation map (where c is the local lattice parameter, and c_{ref} the lattice parameter of a reference region), was performed on small sections of material of about 20 nm size. While investigating the composition profile across the different QWs, we ignored any fluctuations in the plane of these QWs. Therefore, for each section of the material, one deformation profile was recorded across a QW (from bottom to top), with each data point of the profile being the lateral average deformation taken over about 20 nm. Then for each sample, the profiles have been corrected so that the GaN barrier far from the QW undergoes no deformation, *i.e.* $\varepsilon_z = 0$. The profiles were then averaged, using the half-height of the bottom QW interface as the matching point.

3 Results and discussion

3.1 Transmission electron microscopy The structure of the QWs was first investigated by STEM-HAADF and is shown in Fig. 2. As can be seen, 1T growth and Q2T growth result in uniform QW thickness while the 2T QWs exhibit GWWFs [12]. This is explained by the fact that a low temperature GaN cap layer was grown on top of the InGaN QW in order to prevent indium desorption during the temperature ramp. We can also see that in the case of the \sim Q2T growth, which was expected to be the

Table 1 Thickness (t_{InGaN} , t_{GaN}), indium composition (x), characteristic length (d), tail length and segregation efficiency (R) of the samples. Due to the presence of GWWFs, sample 2T cannot be uniquely characterized.

sample	t_{InGaN} (nm)	x (%)	t_{GaN} (nm)	d (nm)	tail length (nm)	R (%)
1T	2.6 ± 0.1	18.9 ± 1	7.1 ± 0.1	0.8	2.1	73
Q2T	2.4 ± 0.1	17.4 ± 1	7.4 ± 0.1	0.4	0.9	52
~Q2T	2.2 ± 0.1	17.5 ± 1	7.5 ± 0.1	0.3	0.8	43
2T	—	—	—	0.2	0.5	23

intermediate method between Q2T and 2T, GWWFs are observed provided the TEM foil is thin enough (Fig. 2(e)). It should be noted that except for sample ~Q2T, the observed QW thickness uniformity (or non-uniformity) was the same whether a very thin or a slightly thicker region of the TEM foil was observed. It was previously reported that the GWWFs arise from long troughs in the QWs which are elongated along a preferential direction, in this case $\langle 11\bar{2}0 \rangle$ [16–18]. However, in the case of sample ~Q2T, unlike sample 2T, no GWWFs could be observed when the TEM foil was relatively thick (but still electron transparent, so possibly about 200 nm as compared to about 100 nm), as shown in Fig. 2(c). This suggests that the troughs inside the ~Q2T-grown QWs are not as elongated as in 2T-grown QWs (pits rather than troughs). The fact that GWWFs in ~Q2T are not the same as in 2T was confirmed by XRD. So far the only unequivocal way to characterize GWWFs is by STEM-HAADF but XRD can give some insight on the presence of GWWFs in a sample. A structure with identical and uniform QWs will have missing or weaker satellite

peaks around the symmetric reflection [14]. However, a structure which exhibits various QW thicknesses, as is the case with GWWFs, will result in no missing or weaker peak. A simple explanation is that a missing/weak peak is representative of one particular QW thickness and in the case of GWWFs we have the superposition of various missing/weak peaks at different positions which eventually results in an overall XRD spectrum with no missing/weak peaks. One can see in Fig. 3 that sample ~Q2T, akin to samples 1T and Q2T, has a missing/weak -5 satellite peak whilst sample 2T only exhibits monotonically weakening peaks. This is consistent with the conclusion from the STEM-HAADF data that sample ~Q2T presents indeed some GWWFs but to a smaller extent than sample 2T.

Figure 4 shows a typical compositional profile across the QW when grown using the Q2T method. This profile is the average of several 20 nm laterally averaged profiles (the dotted lines, corresponding to the standard error of each pixel, are plotted to show the spread of the profiles considered for the average). At first, one can see that the compositional profile is not rectangular for any sample, as might be expected from the growth recipe [10, 11, 19]. For comparison, a rectangular profile corresponding to what is simulated by XRD is superposed on the HRTEM profiles.

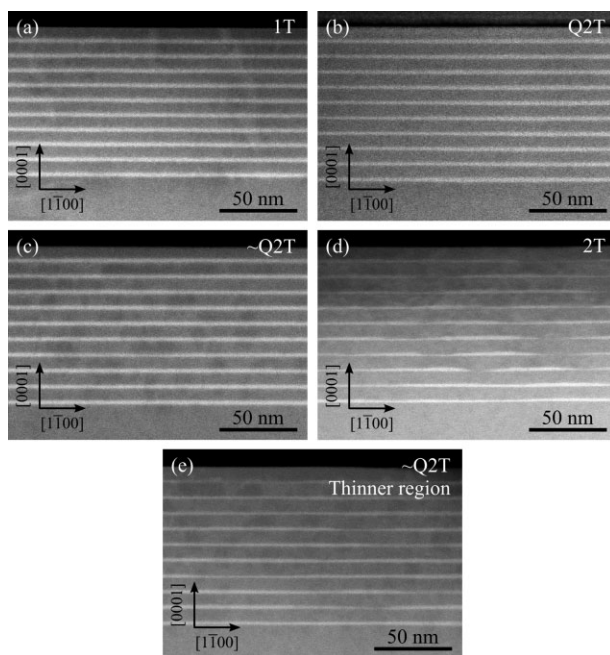


Figure 2 STEM-HAADF images, taken along the $\langle 11\bar{2}0 \rangle$ zone-axis, of samples (a) 1T, (b) Q2T, (c,e) ~Q2T and (d) 2T. The image in (e) is taken in a thinner region of the TEM specimen than the image in (c), and shows GWWFs.

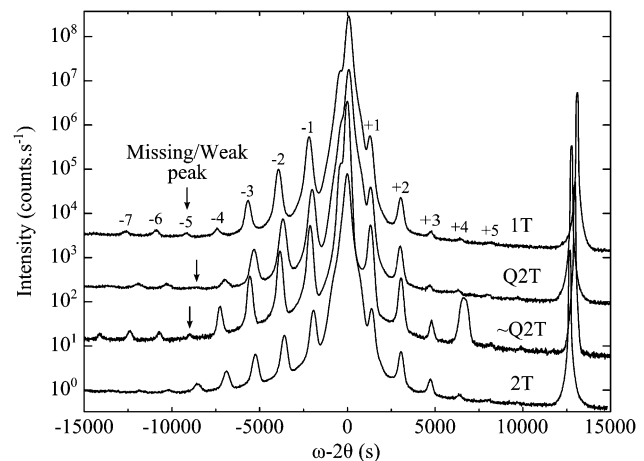


Figure 3 XRD open detector scans taken along the 002 reflection, showing the presence of missing/weaker peaks (indicated by arrows). For comparison of the samples, a vertical offset was employed. The unusually intense peak of the $+4$ satellite peak of sample ~Q2T comes from the aluminum stage of the diffractometer.

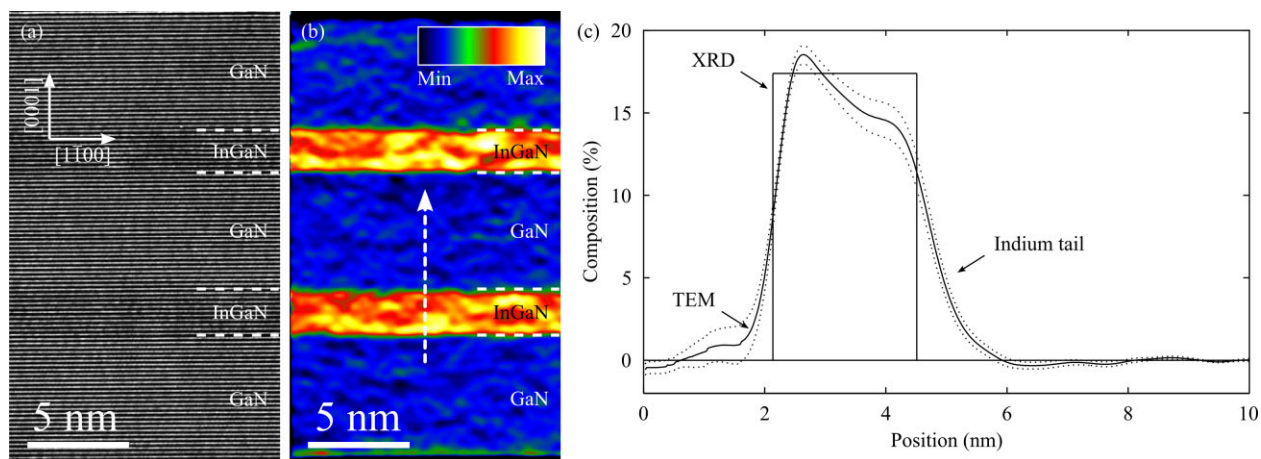


Figure 4 (a) HRTEM image and (b) deformation map of InGaN/GaN QWs of sample Q2T. (c) Composition profile along the growth direction (as arrowed in (b)) and comparison with XRD data (the dotted lines correspond to the standard error).

We can see that both profiles, obtained by geometric phase analysis and XRD, seem to compare well within the error bars (0.6% and 1% for geometric phase analysis and XRD, respectively) thus supporting the reliability of our results. Compared to the nominal growth model, consisting of a rectangular QW with abrupt interfaces, the compositional profiles we obtained exhibit three main features. At the bottom interface of the QW is a peak in indium concentration. Our preliminary results (not shown here) suggest that this bump is mainly due to a higher sensitivity of this interface to electron beam damage. Perhaps, this oversensitivity arises from a slightly higher indium composition in the bottom part of the QW. Above this bump, the composition seems to stabilize to form a plateau of almost constant composition, the value of which seems to agree with our results from XRD. Finally the indium concentration in the upper part of the QW slowly decays, thus forming an indium tail which penetrates into the barrier indicating unintentional indium incorporation during the barrier growth. Such indium incorporation, attributed to indium surface segregation [20], has already been observed in (In,Ga)(As,N) systems grown by molecular beam epitaxy (MBE) [9, 20–23], and also in MOVPE grown structures [9–11, 19, 24, 25]. It should be noted that for 2T samples the compositional profiles were averaged across regions of QWs with identical thicknesses and only the indium tail at the upper interface has been recorded.

The length of the indium tail varied significantly between the four samples. (We should recall that the major difference between these samples, in terms of growth, lies in the thickness of the protective GaN cap layer.) In order to quantify the abruptness of each of the upper interfaces, an exponential fit was applied to the indium tails. As can be seen in Fig. 5, the composition of the indium tails were approximated by a single exponential decay $x(z) = x_0 e^{-z/d}$, where x is the composition, x_0 is the composition of the plateau, z is the position along [0001] ($z = 0$ nm corresponds

to the elbow between the plateau and the tail) and d is the characteristic length of the tail (in nm). Based on this approximation, one can define the length of the indium tail, or depth of indium incorporation into the barrier, as the distance between the end of the QW (position at which $x = x_0/2$) and the composition corresponding to the barrier (position at which $x = 0.6\%$, which is the uncertainty of the geometric phase analysis in this experiment) given by the formula $d(\ln(x_0/0.6) - \ln(2))$. The results are summarized in Table 1. One can see that the indium penetration into the barrier decreases from sample 1T, Q2T, \sim Q2T to 2T indicating that a correlation may exist with the thickness of the low temperature GaN cap layer grown on top of the QW. Computations by Karpov et al. using a rate-equation model which allowed an unsteady-state simulation of indium adatom segregation effects under time-dependent conditions

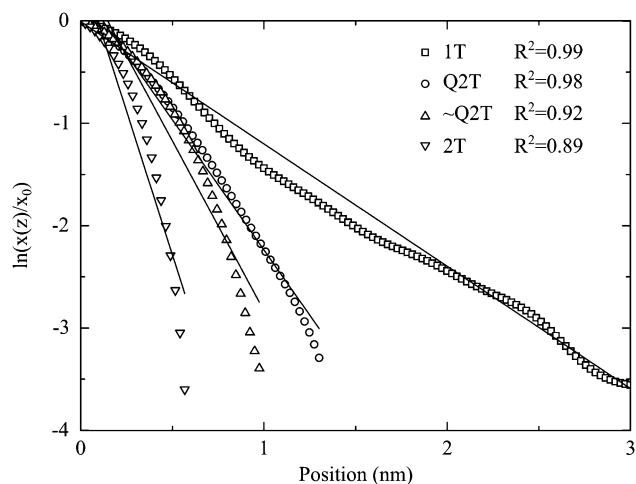


Figure 5 Logarithmic plot of the indium tail for each sample. The plots were fitted by a linear fit, with the coefficients of correlation mentioned in the label.

demonstrated the formation of a compositional tail at the QW top interface [24]. Their model suggests that when the temperature in the reactor increases the surface coverage of indium decreases. In our samples, this result reflects that just before the GaN barrier growth, the indium surface coverage is expected to be higher for sample 1T and Q2T ($T = 756^\circ\text{C}$) than for sample 2T ($T = 852^\circ\text{C}$). Therefore the amount of indium available for incorporation during the growth of the subsequent GaN layers is higher for samples 1T and Q2T than for sample 2T. Consequently, this model predicts a more rapid decay in indium fraction for sample 2T than for sample 1T and Q2T.

Muraki et al. used a simple model to describe the surface segregation of indium, in which a fraction R of the indium present at the n^{th} layer of material is incorporated into the $(n + 1)^{\text{th}}$ layer of material [20] according to the equation:

$$x_{n < N} = x_0(1 - R^n),$$

$$x_{n > N} = x_0(1 - R^N)R^{n-N},$$

where N is the number of monolayers in the QW, x_n is the composition of the n^{th} monolayer and x_0 the nominal composition of the QW. This model has been found successful in describing surface segregation of indium in GaAs grown by MBE [20, 22]. Nevertheless, the method of growth (MOCVD, MBE, etc.) has been shown to affect strongly the segregation of indium [9]. Moreover, in the case of InGaNAs grown by plasma-assisted MBE [23], this model has been found to be unsatisfactory in describing the compositional variation at the interface of the QW. In our samples, we observed that a single exponential decay was a reasonable approximation of the compositional variations at the top QW interface, which means that Muraki et al.'s model [20] seems to apply providing that $R = e^{-c/2d}$, where c is the lattice spacing along the growth direction. The results for the segregation efficiencies for each sample are summarized in Table 1 (assuming $c = c_{\text{GaN}} = 0.51851 \text{ nm}$ [26]). We obtain a segregation efficiency of 73% for sample 1T, which is very similar to the 69% efficiency observed in Ref [9] under similar growth conditions. Nevertheless, the segregation efficiencies for all the other samples are much lower than for sample 1T. If we assume Muraki et al.'s model to be valid, at least for samples 1T and Q2T where a GaN layer is deposited at the same temperature, we should expect the same composition decay observed for sample 1T during the growth of the low temperature capping layer in sample Q2T. Thereafter, the temperature ramp in sample Q2T would be expected to either desorb the indium remaining at the surface, or result in segregation in the following layers with a much lower efficiency. Therefore, the composition in sample 1T should present a single exponential decay, while the composition in sample Q2T should present a first exponential decay during the growth of the cap layer (about 1 nm thick) followed by a change in the slope indicative of the temperature ramp. Instead the

indium tail in sample Q2T has a length similar to the 1 nm thickness of the cap layer, whereas the composition at the beginning of the temperature ramp (*i.e.* at the end of the low temperature capping layer) is expected to be about 4%. From this comment and from the values of R in Table 1, we can point out that the segregation efficiency strongly depends on the growth temperature of the barrier, which reflects the temperature dependence of the indium surfactant layer. It can also be suggested that during the growth of an $(n + 1)^{\text{th}}$ layer at higher temperature (typically during the temperature ramp), indium atoms from layer n , but also $n - 1$, $n - 2$, etc. will diffuse towards the surface, thus changing the R parameter at the QW upper interface.

3.2 Simulation Given that the samples have a different nominal composition and thickness (see Table 1), but also exhibit GWWFs in the case of sample 2T and to a lesser extent, in sample \sim Q2T, a direct comparison of their emission properties would be unhelpful. In order to compare the impact of the indium tail only, a self-consistent Schrödinger–Poisson calculator was employed [13]. The samples modeled here are single QW LEDs consisting of 80 nm of Si-doped GaN with a doping of $4 \times 10^{18} \text{ cm}^{-3}$, followed by a 30 nm undoped GaN layer, an InGaN QW with a nominal thickness of 2.5 nm and nominal composition of 17%, a nominally 7.5 nm GaN barrier and finally a 100 nm thick Mg-doped GaN layer with a doping of $1 \times 10^{17} \text{ cm}^{-3}$. We considered five structures for the simulation, corresponding to the nominally grown LED with a rectangular QW, and LEDs with QWs having indium tails with similar characteristic lengths to those defined in Table 1. The samples will be labeled as “Simulated 1T” ($d = 0.8 \text{ nm}$), “Simulated Q2T” ($d = 0.4 \text{ nm}$), “Simulated \sim Q2T” ($d = 0.3 \text{ nm}$), “Simulated 2T” ($d = 0.2 \text{ nm}$), and “Rectangular” ($d = 0 \text{ nm}$). The QWs were simulated so that the plateau composition x_0 is 17%, and the QW width, measured from the lower interface to the point where the indium composition falls to half of x_0 , is 2.5 nm.

The conduction and valence band energies at equilibrium (when no forward bias is applied) have been calculated for each structure, and are plotted in Fig. 6 for the two extreme cases, *i.e.* Simulated 1T and Rectangular QWs. The electron and hole wavefunctions were superimposed on the conduction and valence band profiles to show the effects on the confinement of carriers inside the QWs. As can be seen, decreasing the abruptness of the upper interface affects the band diagram by reducing the electron energy barrier in the conduction band from 250 meV to approximately zero and decreasing the energy barrier in the valence band by up to 50 meV approximately; consequently reducing the confinement of the carrier wavefunctions within the QW. Under the influence of the built-in electric field in the QW, the electron wavefunction is forced towards the upper interface of the QW while the hole wavefunction towards the lower interface. Therefore, the penetration of the electron wavefunction into the GaN barrier significantly increases as the

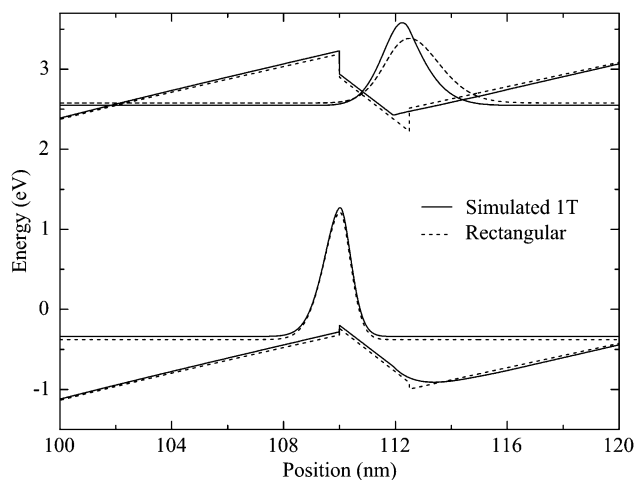


Figure 6 Band diagram and electron–hole wavefunctions of the Simulated 1T structure, with a tail characteristic length $d = 0.8$ nm (solid line), and of the Rectangular structure, with a tail characteristic length $d = 0$ nm (dotted line).

effective barrier height is reduced due to the presence of an indium tail (*i.e.* as d increases), while the hole wavefunction is comparatively unaffected.

Figure 7(a) summarizes the variation in the electron and hole wavefunction overlap as a function of the characteristic indium tail length d at equilibrium. The wavefunction overlap is shown to systematically decrease as the upper QW interface gets smoother, thus reflecting the progressive reduction in confinement of the electron wavefunction demonstrated in Fig. 6. It should also be noted that the decrease in wavefunction overlap is linear for a range of characteristic indium tail lengths from 0.2 nm to 0.8 nm. The observed decrease in wavefunction overlap is expected to reduce the radiative recombination rate within the QW, which may subsequently lead to a reduction in the recombination efficiency due to less effective competition with non-radiative recombination processes. A second point worth noting is the independence of the calculated QW recombination energy on the indium tail, with variations within 4 meV for the simulations of all the experimental structures (*i.e.* all structures except for the Rectangular QW) which suggests that the presence of an indium tail does not significantly influence the emission energy of a QW structure. Finally, in order to characterize the decrease in energy barrier for holes associated with the indium tail, the energy difference at the valence band measured between the bottom of the QW and the minimum in energy above the QW (shown schematically for sample Simulated 1T in Fig. 7(b)) has been recorded. Figure 7(b) presents the evolution of the energy difference with the characteristic length. It can be observed that the energy difference decreases almost linearly for the range of characteristic length considered. We measure a decrease of up to 50 meV of the energy barrier for holes, which may lead to an increase in the hole capture probability into the QW from the GaN barrier. This result suggests that a

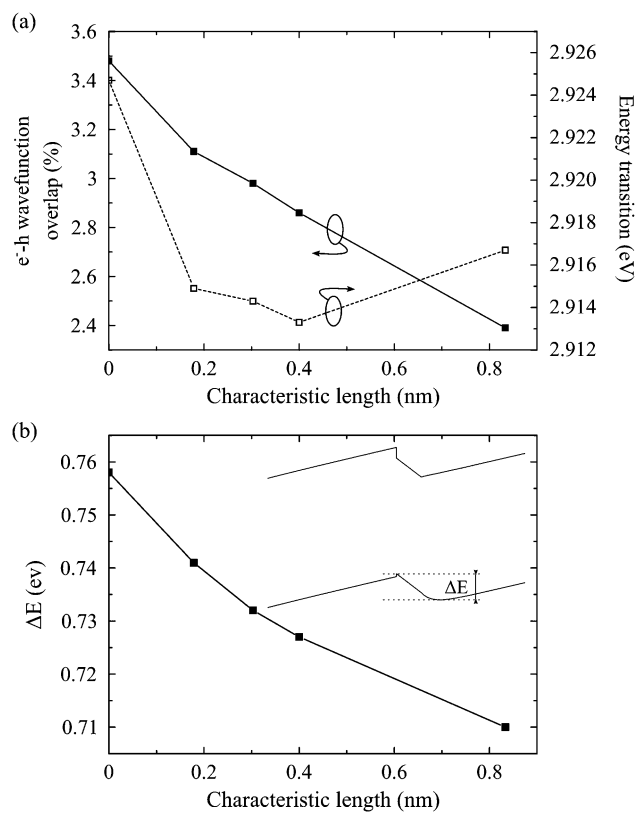


Figure 7 (a) Evolution of the electron–hole wavefunction overlap (filled symbols) and energy transition (open symbols) with the tail characteristic length at equilibrium. (b) Evolution of the hole energy barrier (measured as the difference between the valence band energy at the bottom of the QW and the minimum value of the energy above the QW, as shown here for sample Simulated 1T) with the tail characteristic length at equilibrium.

smoother upper interface may improve the injection of holes in the active region, which has been previously linked to limitations in LED performance [27].

Finally, in Fig. 8 we compare the electron-hole wavefunction overlap for a rectangular QW for a range of thicknesses and alloy compositions. The wavefunction overlaps are normalized with regard to a rectangular QW with composition and thickness of 17% and 2.5 nm, respectively. For comparison the overlaps of Simulated 1T, Simulated Q2T, Simulated \sim Q2T and Simulated 2T are plotted on the graph. It can be observed that the wavefunction overlap decreases with both increasing QW thickness and indium content. From this graph one can assess the impact of the indium tail on the overlap, and in theory, on the radiative recombination rate. For a QW nominally grown with 2.5 nm in thickness and 17% in composition, the indium tail is shown to have the same effect on the wavefunction overlap as an increase of indium composition of up to 3.5%, or an increase in thickness of up to 0.25 nm. In the case of the Simulated 1T, the graded QW upper interface results in a decrease of up to 31% in

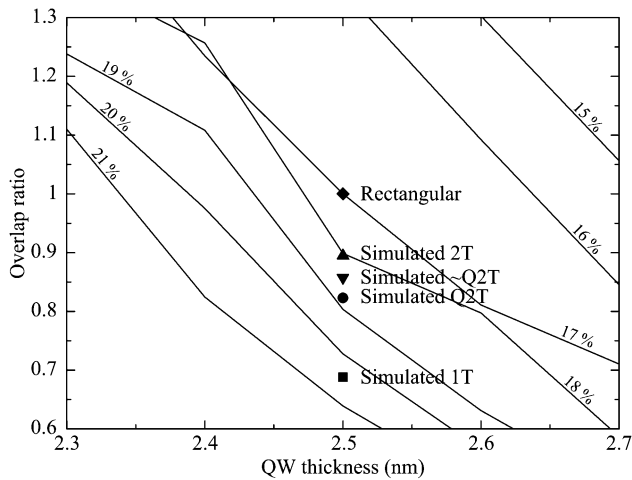


Figure 8 Relative electron–hole wavefunction overlap for rectangular InGa_N QWs with various thickness and composition. The overlaps were normalized relatively to a rectangular QW with composition and thickness of 17% and 2.5 nm, respectively.

wavefunction overlap, while having very little effect on the emission energy of the QW. Unfortunately, it is not possible to differentiate experimentally the three potential causes for decrease in wavefunction overlap, by time-resolved photoluminescence (PL) for example, as any deviation from the nominal configuration of the QW would be within the error bars of the characterization techniques (XRD, TEM and PL).

4 Conclusion Geometric phase analysis has been employed to investigate the impact of the GaN barrier growth technique on the composition profile of InGa_N QWs along the growth direction. We showed that the compositional profiles deviate from their nominal configuration by the presence of an indium tail at the upper interface of the QW. This indium tail, associated with an indium adatom segregation effect, has been shown to strongly depend on the growth method. The effect of this tail has been investigated using a self-consistent Schrödinger–Poisson simulation. For the simulated conditions, a compositionally graded upper interface has been found to result in a decreased electron–hole wavefunction overlap of up to 31% compared to QW with sharp interfaces, leading to a decrease in radiative recombination rate while the QW emission energy remains unchanged. In order to maximize the efficiency of a QW structure, it is therefore important to grow the active region using a growth method which leads to QW interfaces which are as abrupt as possible.

The results of this experiment find applications in every study where the emission properties of a device are correlated to a particular active region design [3–5, 28]. This study is of particular interest for InGa_N/GaN MQW or superlattice structures in which the individual layer thicknesses are less than 2 nm. Disregarding graded interfaces would lead to serious underestimation of the

effective QW thickness (and consequently to an overestimation of the oscillator strength in the QWs). Also, the average bandgap of the barrier would be decreased, thus leading to a reduced carrier confinement in the active region.

Acknowledgements The authors acknowledge support from the EPSRC under EP/H0495331.

References

- [1] S. Nakamura, T. Mukai, and M. Senoh, *Appl. Phys. Lett.* **64**, 1687 (1994).
- [2] C. J. Humphreys, *MRS Bull.* **33**, 459 (2008).
- [3] L. Zhang, R. R. Lieten, M. Latkowska, M. Baranowski, R. Kudrawiec, K. Cheng, H. Liang, and G. Borghs, *Jpn. J. Appl. Phys.* **52**, 08JL10 (2013).
- [4] R. Vaxenburg, E. Lifshitz, and A. L. Efros, *Appl. Phys. Lett.* **102**, 031120 (2013).
- [5] Z. Yang, R. Li, Q. Wei, T. Yu, Y. Zhang, W. Chen, and X. Hu, *Appl. Phys. Lett.* **94**, 061120 (2009).
- [6] E. V. Yakovlev, A. S. Segal, K. A. Bulashevich, S. Y. Karpov, and R. A. Talalaev, *Jpn. J. Appl. Phys.* **52**, 08JB15 (2013).
- [7] V. Hoffmann, A. Mogilatenko, C. Netzel, U. Zeimer, S. Einfeldt, M. Weyers, and M. Kneissl, *J. Cryst. Growth* **391**, 46 (2014).
- [8] H. Zhao, G. Liu, J. Zhang, J. D. Poplawsky, V. Dierolf, and N. Tansu, *Optics Express* **19**, A991 (2011).
- [9] V. Potin, E. Hahn, A. Rosenauer, D. Gerthsen, B. Kuhn, F. Scholz, A. Dussaigne, B. Damilano, and N. Grandjean, *J. Cryst. Growth* **262**, 145 (2004).
- [10] T. Mehrtens, M. Schowalter, D. Tytko, P. Choi, D. Raabe, L. Hoffmann, H. Jonen, U. Rossow, A. Hangleiter, and A. Rosenauer, *Appl. Phys. Lett.* **102**, 132112 (2013).
- [11] L. Hoffmann, H. Bremers, H. Jonen, U. Rossow, M. Schowalter, T. Mehrtens, A. Rosenauer, and A. Hangleiter, *Appl. Phys. Lett.* **102**, 102110 (2013).
- [12] N. K. Van der Laak, R. A. Oliver, M. J. Kappers, and C. J. Humphreys, *Appl. Phys. Lett.* **90**, 121911 (2007).
- [13] S. Birner, T. Zibold, T. Andlauer, T. Kubis, M. Sabathil, A. Trellakis, and P. Vogl, *IEEE Trans. Electron Devices* **54**, 2137 (2007).
- [14] M. E. Vickers, M. J. Kappers, T. M. Smeeton, E. J. Thrush, J. S. Barnard, and C. J. Humphreys, *J. Appl. Phys.* **94**, 1565 (2003).
- [15] M. J. Hytch, E. Snoeck, and R. Kilaas, *Ultramicroscopy* **74**, 131 (1998).
- [16] N. Jouvet, M. J. Kappers, C. J. Humphreys, and R. A. Oliver, *J. Appl. Phys.* **113**, 063503 (2013).
- [17] N. K. Van der Laak, R. A. Oliver, M. J. Kappers, and C. J. Humphreys, *J. Appl. Phys.* **102**, 013513 (2007).
- [18] R. A. Oliver, M. J. Kappers, and C. J. Humphreys, *Phys. Status Solidi C* **5**, 1475 (2008).
- [19] G. Ju, Y. Honda, M. Tabuchi, Y. Takeda, and H. Amano, *J. Appl. Phys.* **115**, 094906 (2014).
- [20] K. Muraki, S. Fukatsu, Y. Shiraki, and R. Ito, *Appl. Phys. Lett.* **61**, 557 (1992).
- [21] A. Dussaigne, B. Damilano, N. Grandjean, and J. Massies, *J. Cryst. Growth* **251**, 471 (2003).
- [22] T. Mehrtens, K. Muller, M. Schowalter, D. Hu, D. M. Schaadt, and A. Rosenauer, *Ultramicroscopy* **131**, 1 (2013).

- [23] E. Luna, F. Ishikawa, P. D. Batista, and A. Trampert, *Appl. Phys. Lett.* **92**(14), 141913 (2008).
- [24] S. Y. Karpov, R. A. Talalaev, I. Y. Evstratov, and Y. N. Makarov, *Phys. Status Solidi A* **192**, 417 (2002).
- [25] M. J. Galtrey, R. A. Oliver, M. J. Kappers, C. J. Humphreys, P. H. Clifton, D. Larson, D. W. Saxey, and A. Cerezo, *J. Appl. Phys.* **104**, 013524 (2008).
- [26] M. E. Vickers, J. L. Hollander, C. McAleese, M. J. Kappers, M. A. Moram, and C. J. Humphreys, *J. Appl. Phys.* **111**, 043502 (2012).
- [27] J. Xie, X. Ni, Q. Fan, R. Shimada, U. Ozgur, and H. Morkoc, *Appl. Phys. Lett.* **93**, 121107 (2008).
- [28] R. J. Choi, Y. B. Hahn, H. W. Shim, M. S. Han, E. K. Suh, and H. J. Lee, *Appl. Phys. Lett.* **82**, 2764 (2003).